First Observations of a Polynya in the Last Ice Area North of Ellesmere Island

G. W. K. Moore[1], Stephen Howell[2], and Michael Brady[3]

[1]University of Toronto
[2]Environment and Climate Change Canada
[3]Environment Canada

November 22, 2022

Abstract

The area to the north of Ellesmere Island and Greenland contains the Arctic's thickest ice and it is predicted to be the last to lose its perennial ice, thus providing an important refuge for ice-dependent species. There is however evidence that this Last Ice Area is, like the entire Arctic, undergoing rapid changes that may reduce its suitability as a refuge. During May 2020, a polynya developed to the north of Ellesmere Island in a region where there are no reports of a previous development during May. We use a variety of remotely sensed data as well as atmospheric models to document the evolution and the dynamics responsible for the polynya. In particular, we argue that anomalously strong divergent winds associated with an intense and long-lived Arctic anti-cyclone contributed to the development of the polynya as well as a similar previously unreported event in May 2004.

First Observations of a Polynya in the Last Ice Area North of Ellesmere Island

G. W. K. Moore[1,2], S. E. L. Howell[3], and M. Brady[3]

[1]Department of Physics, University of Toronto, Toronto, Ont. Canada

[2]Department of Chemical and Physical Sciences, University of Toronto Mississauga, Mississauga, Ont. Canada

[3]Climate Research Division, Environment and Climate Change Canada, Toronto, Ont. Canada

Corresponding author: G.W.K. Moore (gwk.moore@utoronto.ca)

Key Points:

- During May 2020, a polynya with an area in excess of 3,000 km^2 developed in the Last Ice Area to the north of Ellesmere Island.
- There are no previous records of a polynya previously forming in this region during May.
- We argue that strong divergent winds associated with an intense anti-cyclone were responsible for the development.

Abstract

The area to the north of Ellesmere Island and Greenland contains the Arctic's thickest ice and it is predicted to be the last to lose its perennial ice, thus providing an important refuge for ice-dependent species. There is however evidence that this Last Ice Area is, like the entire Arctic, undergoing rapid changes that may reduce its suitability as a refuge. During May 2020, a polynya developed to the north of Ellesmere Island in a region where there are no reports of a previous development during May. We use a variety of remotely sensed data as well as atmospheric models to document the evolution and the dynamics responsible for the polynya. In particular, we argue that anomalously strong divergent winds associated with an intense and long-lived Arctic anti-cyclone contributed to the development of the polynya as well as a similar previously unreported event in May 2004.

Plain Language Summary

A polynya is an area of open water in a region that is normally ice covered. The absence of ice allows for the exchange of energy between the atmosphere and ocean as well as supporting a complex ecosystem. The Last Ice Area (LIA) is the region north of Greenland and Ellesmere Island that contains the Arctic's oldest and thickest ice. It is also predicted to be the last region to lose its multi-year ice thus providing a refuge for ice dependent species. There is evidence that the LIA is also experiencing a thinning ice cover that may reduce its reliance to ice loss. In this paper, we describe the development of a polynya during May 2020 to the north of Ellesmere Island where such events have not been previously observed. We argue that anomalous winds associated with an intense Arctic anti-cyclone were responsible for the event. We also identify a similar but smaller event during May 2004 that was associated with stronger wind forcing as compared to the 2020 event. We argue that is consistent with what would be expected to occur as a result of thinning ice. This suggests that such events may become more common in the future.

1 Introduction

The Arctic Ocean's oldest and thickest ice lies along an arc to the north of Greenland and the Canadian Arctic Archipelago (Bourke & Garrett, 1987; Maslanik et al., 2011). Over the period 1979-2019, ice in this area has an average thickness in excess of 4m and an average age in excess of 5 years (Moore et al., 2019). Climate models suggest that this area will be the last to lose it multi-year ice (Laliberté et al., 2016; Notz & Community, 2020) thus providing a refuge for ice dependent species and, this region is now referred to as the Last Ice Area or the LIA, (Pfirman, 2009; Moore et al., 2019). Indeed, the Government of Canada has recently established the Tuvaijuittuq, Inuktitut for the 'the place where the ice never melts' Marine Protected Area north of Ellesmere Island to help conservation efforts in the LIA (Government_of_Canada, 2019).

There is however evidence that the LIA is also undergoing rapid changes and is not as homogeneous a region as previously thought (Loewen & Michel, 2018; Moore et al., 2019). For example, the loss of LIA's ice mass is twice the basin average while ice motion in the western LIA, to the north of the Canadian Arctic Archipelago, is increasing at twice the basin average (Moore et al., 2019). In addition, there has been a recent doubling in the ice area flux along Nares Strait, the major pathway along which multi-year ice leaves the LIA as well as a weakening in the ice arches along the strait that modulate this export (Moore & McNeil, 2018; Moore et al., 2021).

This suggests that the LIA may not be as resilient to climate change as previously thought (Moore et al., 2019; Schweiger et al., 2021).

As is the case in other regions (Trenberth et al., 2015), it remains a challenge in the Arctic to distinguish the impacts of inter-annual variability from those associated with a changing climate. During February 2018, a polynya formed in the Wandel Sea in the eastern LIA, a region where polynyas have not been previously observed (Moore et al., 2018). It was argued that anomalous wind forcing rather than thinning ice was responsible for the development of the polynya and that even with ice thicknesses typical of the region in the late 1970s, the polynya would still have developed. August 2020 saw record low ice concentrations in the Wandel Sea that resulted in the German Icebreaker Polarstern transiting through the region, that typically has some of the thickest ice in the Arctic, as part of the MOSAiC experiment (Schweiger et al., 2021). Schweiger et al.(2021) argued that this anomaly was the result of the long-term trend towards a thinner ice pack in the region as well as advection of ice out of the region by anomalous winds associated with an anti-cyclonic circulation across the Arctic and summer melt.

In this paper, we report on a polynya that developed within the LIA to the north of Ellesmere Island during May 2020. Flaw leads, elongated regions of open water that develop along the interface between land fast and pack ice (Barber & Massom, 2007) are common in the region. Indeed Peary's progress towards the North Pole during February and March 1909 was delayed as a result of a large flaw lead that developed north of Ellesmere Island (Peary, 1910). However, the development of a polynya in this region has never been reported previously. We use a variety of remotely sensed sea ice products as well as atmospheric model data to document the evolution of the polynya and show that it was most likely the result of anomalously strong winds associated with an intense Arctic anti-cyclone. We also show that a similar event also occurred in May 2004 under similar atmospheric flow.

2 Data

A variety of remotely sensed products were used to characterize the development of the May 2020 polynya and place this development in a longer-term context. True-color satellite images with a resolution of 250m from the MODIS instrument (Hillger et al., 2011) will be used to visualize the development of the polynya. Sea ice concentrations derived from AMSR-(E/2) passive microwave data using the ARTIST sea ice (ASI) algorithm will be to characterize and quantify the polynya (Spreen et al., 2008). During May, the data is available daily at a spatial resolution of 3.125km from, with some disruptions, 2003-2020. The high spatial resolution of this dataset, resulting from the presence of 89Ghz channel on the AMSR instrument, was critical to resolving the polynya, something not possible with the lower resolution sea ice concentration datasets, such as the National Snow and Ice Data Center's Climate Data record (Peng et al., 2013). Sequential pairs of Synthetic Aperture Radar (SAR) imagery with a resolution of 100m from the RADARSAT-1 satellite (Singhroy & Charbonneau, 2014) and with a resolution of 40m from the Sentinel-1 satellite (Torres et al., 2012) were used within the Environment and Climate Change Canada Automated Sea Ice Tracking System (ECCC-ASITS) that uses the Komarov and Barber (2013) automated tracking algorithm.

The ERA5 reanalysis (Hersbach et al., 2020) will be used to characterize the surface meteorology during the life-cycle of the polynya. The ERA5 is available at a one hour temporal resolution and an ~30km horizontal resolution from 1950-2020. The ERA5 is based on the

European Centre for Medium-Range Weather Forecasts' (ECMWF) Integrated Forecast System (Hersbach et al., 2020). The current operational analysis at the ECMWF is available at a 6 hour temporal resolution and a horizontal resolution of ~ 9km from 2016 onwards (Holm et al., 2016). The operational analysis, referred to as the ECOA, shares many of the same parameterizations with the ERA5 and so it can be used to assess the impact that model resolution has on the representation of high impact meteorological events.

3 Results

The polynya that is of interest developed to the north of Ellesmere Island in a region of climatologically thick ice (Fig 1). MODIS imagery indicated that the polynya was preceded by the occurrence of several large meridionally oriented leads on May 13 2020 to the west of 80^{o}W (Fig 1b). One day later on the 14th (Fig 1c), the complex had evolved to include a flaw lead along the coast that was associated with a large lead that extended northwards of 84^{o}N along 75^{o}W. The flaw lead and its northwards extension into the pack was ~500km long and at its widest was ~10km wide. On the 15th (Fig 1d), this lead continued to evolve reaching a maximum width in excess of 30km. On subsequent days, cloudy skies in the region restricted the ability to visualize the development of this feature using MODIS imagery. On May 28 (Fig 1e), the lead complex and polynya had closed.

Quantitative information on the polynya's evolution and the statistics for open water in the area of interest is provided by the ASI dataset. The initial development of the feature of interest, on May 13-15 (Fig 2a-c) is consistent with the visible imagery shown in Figure 1. By May 19 (Fig 2d), a quasi-elliptical polynya had evolved out of the elongated lead present on the 15th (Fig 1d and Fig 2c). The polynya had a major axis of ~100km and a minor axis of ~30km. Over the next few days, the polynya retained its shape (Fig 2e) before finally closing on the 28th (Fig 2f).

The time series of the area of open water in the region of interest during May 2020 (Fig 2g) provides additional information on the evolution of the polynya. The rapid opening of the polynya on May 15th is evident as well as its sudden closing on May 26. Statistics on the area of open water in the region, as determined for the period 2003-2021, indicate that this event was clearly anomalous with the area of open water far exceeding two standard deviations above the mean for this period of the year.

A longer-term context for the unique nature of the May 2020 event is provided by the monthly mean area of open water in the area of interest during May for the entire period of the ASI dataset, 2003-2021 (Fig 2h). Typically the area of open water during May in the region is less than 160km^2. May 2020 is the only year in which the area of open water exceeds 2 standard deviations above the mean. May 2004 is the only other year where the area of open water exceeded 1 standard deviations above the mean. Supplementary Figure 1 shows that this event also evolved out of a flaw lead but did not extend as far north as the 2020 event. There also appears to a tendency towards larger openings recently. For example, the years with the 3rd, 4th and 5th largest areas of open water all occurred after 2014.

Figure 3 provides information on the sea ice motion derived from the Sentinel-1 SAR imagery during May 2020. During the period of the polynya's opening, May 14 and 15 (Fig 3a&b), there is a marked difference in ice motion to the east and west of the area where the polynya developed. In particular, to the east of ~75° W, there is little or no evidence of ice motion, while to the west, the ice is moving towards the southwest with speeds in excess of 15 km/day. A similar pattern of divergent ice motion occurred during the May 2004 event as well (Supp Fig 1). The time series of the components of the ice motion, derived from all the available Sentinel-1 SAR data for May 2020 (Fig 3c&d), for the two halves of the region of interest, i.e. east and west of 75°W, confirm the contrast in the mobility of the ice. In addition, one can see that the period of large ice motion is confined to the 14th and 15th, the time that the polynya was opening up (Fig 2g). After the opening and up to May 23rd, divergence in ice motion remained with southwestward motion to the west of 75°W. After this time, the direction of the motion reversed contributing to the closing of the polynya on the 26th.

The period of the polynya development during May 2020 was characterized by high sea-level pressures, as compared to climatology (Supp Fig 2) in the western Arctic that were associated with a long-lived anti-cyclone that propagated across the Arctic Ocean (Fig 4a&b). On the day that the polynya opened - May 15, 2020 - the location and strength of the anti-cyclone was such as to result in strong southwesterly flow across the region of interest (Fig 4b). The center pressure of the system was identified for the period of its existence as a well-defined circulation system, 11 GMT on May 11 to 21 GMT on May 16 (Fig 4c). The anti-cyclone reached is maximum strength on the 14th and 15th, the period during which the polynya opened (Fig 4g).

To place the development of this anti-cyclone into a longer-term perspective, the maximum sea-level pressure within a 500km radius of the system's center along its track was determined for each year from 1950 to 2020. These values were used to define the mean and standard deviation of the sea-level pressure along this track. This climatology clearly indicates that during the sea-level pressures associated with the May 2020 anti-cyclone were two standard deviations above the mean.

Considering the region of interest, the sea-level pressure and 10m wind fields at 00 GMT on May 14 and 15 as represented in the ERA5 reanalysis and the ECOA (Fig 5a-d) show the presence of northeasterly flow along the northern coast of Ellesmere Island that is the result of the pressure gradient associated with the anti-cyclone identified above. A ridge that developed over the eastern half of the region of interest contributed to the pronounced zonal gradient in 10m windspeed. The 10m wind speeds were higher and this gradient more pronounced in the higher spatial resolution ECOA product as compared to the ERA5 reanalysis. Information on the extent of open water associated with the flaw lead and polynya are also shown and one can see that these features are generally aligned with the region where there is an acceleration in the 10m wind speed.

Finally, time series of the components of the 10m wind averaged over the region of interest (Fig 5e-f), clearly show the elevated northwesterly winds during the period of the polynya's opening on the 14th and 15th. A comparison with the climatology shows that the zonal component of the 10m wind during the period of the polynya's opening exceeded the mean by two standard deviations while the meridional component exceeded the mean by standard deviation.

Supplementary Figure 3 shows that a similar synoptic circulation and 10m wind speed evolution also occurred during the May 2004 event.

4 Conclusions

Flaw leads are known to develop throughout the LIA (Peary, 1910; Barber & Massom, 2007). Apart from a polynya that developed in February 2018 over the Wandel Sea on the eastern boundary of the LIA (Moore et al., 2018), there have been no reports of the formation of polynyas, especially to the north of Ellesmere Island in the center of the LIA. In this paper, we describe such a development during May 2020.

Visible satellite imagery (Fig 1b-e) as well as sea ice concentration derived from passive microwave satellite data (Fig 2a-f) both indicate that the polynya was preceded by the formation of an elongated flaw lead to the west of 75°W that developed on May 14 2020. A day later on the 15th, the flaw lead began evolve into a polynya that had an area of ~2,000-3,000 km^2 and that persisted for 10 days before closing on the 26th. At its maximum extent, it was elliptical in shape with a major axis of ~100km and a minor axis of ~30km.

Based on sea ice concentration from 2003-2020, this region does not typically have more than ~160km^2 of open water and the 2020 event exceeded the mean by many standard deviations (Fig 2g). Based on monthly mean values over the period of the ASI dataset, 2003-2020, this was the largest area of open water on record and exceeded the monthly mean climatology by more than 2 standard deviations. A smaller event that exceeded the monthly mean climatology by more than 1 standard deviation occurred in 2004. The evolution of this event was similar to that in 2020 with exception that it did not extend as far north (Supplementary Figure 1).

Ice motion data derived from Sentinel-1 SAR imagery (Fig 3) showed that the polynya developed along the boundary between stationary ice to the east and rapidly moving ice to the west. During the ~2 day transition from lead to polynya, the ice pack was moving with speeds up to 20 km/day, a speed consistent with the polynya's minor axis of ~30 km.

The region of interest is situated with a saddle point in the climatological sea-level pressure field resulting in low wind speeds and ice motion (Supp Fig 2). The development of both the 2020 and 2004 events were associated with intense and long-lived Arctic anti-cyclones, with maximum sea-level pressures of ~1048mb (Fig 4a&b; Supp Fig 3). In the case of the 2020 event, the central pressure of the anti-cyclone exceeded climatology by more than 2 standard deviations. Along the coast of northern Ellesmere Island, the impact of the anti-cyclones were strong southwesterly wind with windspeeds of up to 16 m/s that exceeded the mean by over 2 standard deviations (Fig 5 and Supp Fig 3). In both cases, the presence of a ridge over the eastern half of the region of interest resulted in a zonal gradient in wind speed, with higher wind speeds to the west, that aligned with the location of the polynya development. The ECOA product with its horizontal resolution of ~9km, was better able to represent this gradient as compared to the ERA5 reanalysis with its horizontal resolution of ~30km.

This east-west gradient in wind speed and its associated divergence is most likely the reason of the development of the polynya. The thinner ice to the west of the region of interest (Fig 1a) also contributed to the development. It is interesting to note that wind speeds were higher during the 2004 event and yet the resulting polynya was smaller than that in 2020 (Fig 2g; Supp Fig 1a). A possible explanation is that the trend towards thinner ice that is occurring within the LIA (Moore et al., 2019) contributed to the larger polynya in 2020 despite weaker forcing. In this regard, it was also noted that there is a tendency for larger areas of open water in the region during May since 2014. In this respect, it appears that these events during May are fundamentally different from the February 2018 Wandel Sea polynya, where wind dynamics alone and not thinning ice were responsible for that development.

The May 2020 event, when compared to that in May 2004, provides additional evidence as to the changing nature of sea ice within the LIA as well as the importance of synoptic weather systems in forcing extreme ice events in the region.

Acknowledgments

GWKM would like to acknowledge the support of the Natural Sciences and Engineering Research Council of Canada. Sentinel-1 imagery (https://scihub.copernicus.eu/dhus/#/home) and the ERA5 data (https://cds.climate.copernicus.eu/#!/home) were provided by the Copernicus Program. The ASI sea ice concentration data was provided by the University of Bremen (https://seaice.uni-bremen.de/sea-ice-concentration/amsre-amsr2/). The ECOA data was provided by the National Center for Atmospheric Research (https://rda.ucar.edu). RADARSAT-1 imagery were provided by the Alaska Satellite Facility (https://asf.alaska.edu). The authors do not have any conflicts of interest with respect to this work.

References

Barber, D. G., & Massom, R. A. (2007). The role of sea ice in Arctic and Antarctic polynyas. *Elsevier Oceanography Series, 74*, 1-54.

Bourke, R. H., & Garrett, R. P. (1987). Sea ice thickness distribution in the Arctic Ocean. *Cold Regions Science and Technology, 13*(3), 259-280. http://www.sciencedirect.com/science/article/pii/0165232X87900073

Government_of_Canada. (2019). *Report on the designation of the Tuvaijuittuq Marine Protected Area*. Retrieved from Ottawa: https://www.dfo-mpo.gc.ca/oceans/publications/tuvaijuittuq/designation/index-eng.html

Hersbach, H., Bell, B., Berrisford, P., Hirahara, S., Horányi, A., Muñoz-Sabater, J., et al. (2020). The ERA5 global reanalysis. *Quarterly Journal of the Royal Meteorological Society, 146*(730), 1999-2049.

Hillger, D. W., Grasso, L., Miller, S. D., Brummer, R., & DeMaria, R. J. (2011). Synthetic advanced baseline imager true-color imagery. *Journal of Applied Remote Sensing, 5*(1), 053520.

Holm, E. V., Forbes, R., Lang, S., Magnusson, L., & Malardel, S. (2016). New model cycle brings higher resolution *ECMWF Newsletter, 147*.

Komarov, A. S., & Barber, D. G. (2013). Sea ice motion tracking from sequential dual-polarization RADARSAT-2 images. *IEEE Transactions on Geoscience and Remote Sensing, 52*(1), 121-136.

Laliberté, F., Howell, S. E. L., & Kushner, P. J. (2016). Regional variability of a projected sea ice-free Arctic during the summer months. *Geophysical Research Letters, 43*(1), 256-263. https://agupubs.onlinelibrary.wiley.com/doi/abs/10.1002/2015GL066855

Loewen, T. N., & Michel, C. (2018). *Proceedings of the Multidisciplinary Arctic Program (MAP) – last ice: science planning workshop, January 16-17, 2018*. Retrieved from

Maslanik, J., Stroeve, J., Fowler, C., & Emery, W. (2011). Distribution and trends in Arctic sea ice age through spring 2011. *Geophysical Research Letters, 38*(13). https://doi.org/10.1029/2011GL047735

Moore, G., Howell, S., Brady, M., Xu, X., & McNeil, K. (2021). Anomalous collapses of Nares Strait ice arches leads to enhanced export of Arctic sea ice. *Nature Communications, 12*(1), 1-8.

Moore, G., Schweiger, A., Zhang, J., & Steele, M. (2018). What Caused the Remarkable February 2018 North Greenland Polynya? *Geophysical Research Letters*.

Moore, G., Schweiger, A., Zhang, J., & Steele, M. (2019). Spatiotemporal variability of sea ice in the arctic's last ice area. *Geophysical Research Letters, 46*(20), 11237-11243.

Moore, G. W. K., & McNeil, K. (2018). The Early Collapse of the 2017 Lincoln Sea Ice Arch in Response to Anomalous Sea Ice and Wind Forcing. *Geophysical Research Letters, 45*(16), 8343-8351. https://doi.org/10.1029/2018GL078428

Notz, D., & Community, S. (2020). Arctic sea ice in CMIP6. *Geophysical Research Letters, 47*(10), e2019GL086749.

Peary, R. E. (1910). The North Pole/by Robert E. Peary; with an introd. by Theodore Roosevelt.

Peng, G., Meier, W. N., Scott, D. J., & Savoie, M. H. (2013). A long-term and reproducible passive microwave sea ice concentration data record for climate studies and monitoring. *Earth Syst. Sci. Data, 5*(2), 311-318. https://essd.copernicus.org/articles/5/311/2013/

Pfirman, S. (2009). The last arctic sea ice refuge. *The Circle, 4*, 6-8. https://web.law.columbia.edu/sites/default/files/microsites/climate-change/files/Arctic-Resources/Sea-Ice-Refuge/Pfirman%20article%20the%20circle.pdf

Schweiger, A. J., Steele, M., Zhang, J., Moore, G. W. K., & Laidre, K. L. (2021). Accelerated sea ice loss in the Wandel Sea points to a change in the Arctic's Last Ice Area. *Communications Earth & Environment, 2*(1), 122. https://doi.org/10.1038/s43247-021-00197-5

Singhroy, V., & Charbonneau, F. J. (2014). RADARSAT: Science and applications. *Physics in Canada, 70*(4).

Spreen, G., Kaleschke, L., & Heygster, G. (2008). Sea ice remote sensing using AMSR-E 89-GHz channels. *Journal of Geophysical Research: Oceans, 113*(C2). http://dx.doi.org/10.1029/2005JC003384

Torres, R., Snoeij, P., Geudtner, D., Bibby, D., Davidson, M., Attema, E., et al. (2012). GMES Sentinel-1 mission. *Remote Sensing of Environment, 120*, 9-24. https://www.sciencedirect.com/science/article/pii/S0034425712000600

Trenberth, K. E., Fasullo, J. T., & Shepherd, T. G. (2015). Attribution of climate extreme events. *Nature Climate Change, 5*(8), 725-730.

Figure 1) Regional setting for and MODIS imagery of the May 2020 polynya event. a) Climatological mean sea ice thickness (m) during April 2002-2020 from the merged AWI CS2-SMOS dataset with the region of interest indicated by the polygon. MODIS visible imagery in the region of interest on May: b)13; c) 14; d) 15; and e) 28 2020.

Figure 2) Evolution of sea ice during the May 2020 polynya event. Sea ice concentration (%) on May: a)13; b) 14; c) 15; d) 19; e) 22 and f) 28 2020. g) Time series of the area of open water (103 km2) in the region of interest during May 2020. h) Time series of the monthly mean area of open water (103 km^2) in the region of interest during May 2003-2021. In g) and h), the climatology based on 2003-2021.

Figure 3) Sentinel-1 SAR imagery and ice motion during the May 2020 polynya event. SAR imagery and ice motion (km/day) on May: a) 14 and b) 15 2020. Time series of the: c) zonal and d) meridional components of the ice motion (km/day) over eastern (blue curves) and western (red curves) halves of the region of interest during May 2020.

Figure 4) Evolution of the synoptic-scale circulation over the Western Arctic Ocean during the May 2020 polynya event. Sea-level pressure (mb-contours), 10m winds (m/s-vectors) and 10m wind speed (m/s-shading) from the ERA5 reanalysis at 00 GMT on May: a) 11 and b) 15 2020. c) The time series (black curve) of the central pressure of the high-pressure system identified in a) and b) with the climatology (blue curves) based all grid points within 500 km of the center of the high-pressure system during the period 1950-2020. In a) and b), the region of interest is indicated by the polygon.

Figure 5) Evolution of the mesoscale circulation during the May 2020 polynya event. The sea-level pressure (mb-contours), the 10m wind (m/s-vectors) and the 10m wind speed (m/s shading) at 00 GMT May 14 2020 from the: a) ERA and b) ECOA and at 00 GMT May 15 2020 from the: c) ERA5 reanalysis and d) ECOA. Also shown with the white contours is the 80% sea ice concentration isocontour from the ASI dataset. The time series of the: a) zonal and c) meridional components of the 10m wind from the ERA5 reanalysis during May 2020 for the oceanic portion of the region of interest. The climatology is based on 1950-2020.

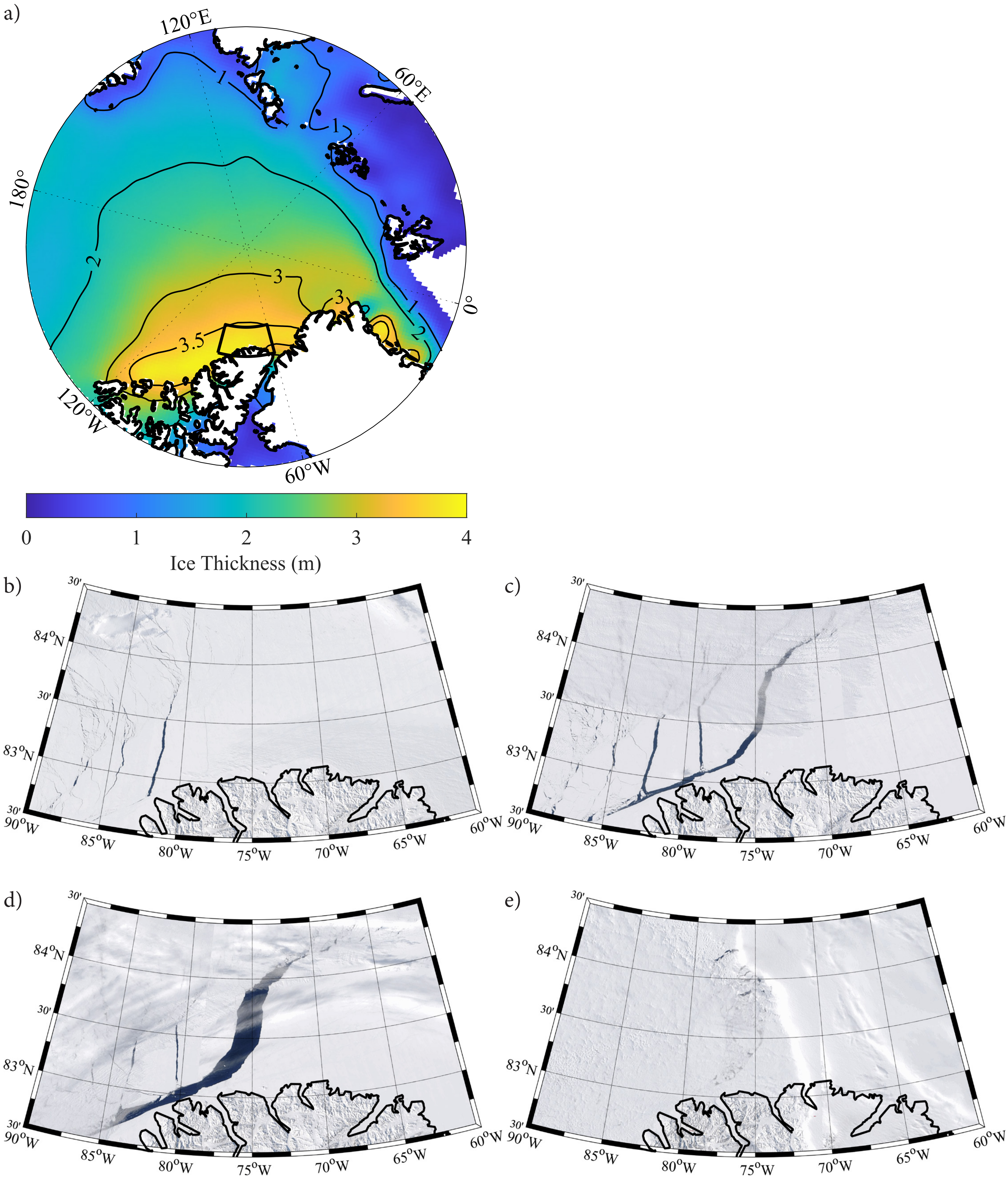

Figure 1) Regional setting for and MODIS imagery of the May 2020 polynya event. a) Climatological mean sea ice thickness (m) during April 2002-2020 from the merged AWI CS2-SMOS dataset with the region of interest indicated by the polygon. MODIS visible imagery in the region of interest on May: b)13; c) 14; d) 15; and e) 28 2020.

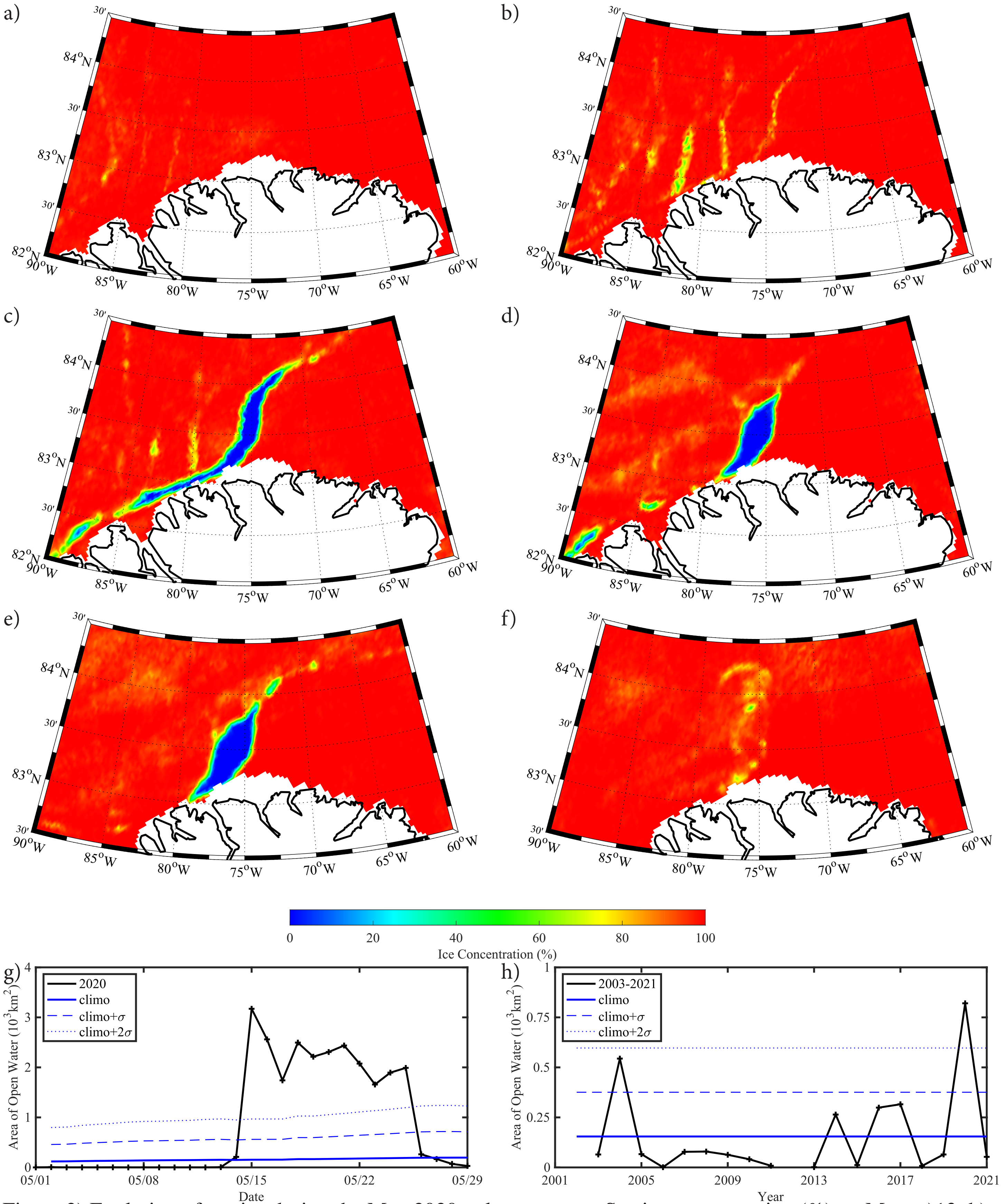

Figure 2) Evolution of sea ice during the May 2020 polynya event. Sea ice concentration (%) on May: a)13; b) 14; c) 15; d) 19; e) 22 and f) 28 2020. g) Time series of the area of open water (103 km2) in the region of interest during May 2020. h) Time series of the monthly mean area of open water (103 km2) in the region of interest during May 2003-2021. In g) and h), the climatology based on 2003-2021.

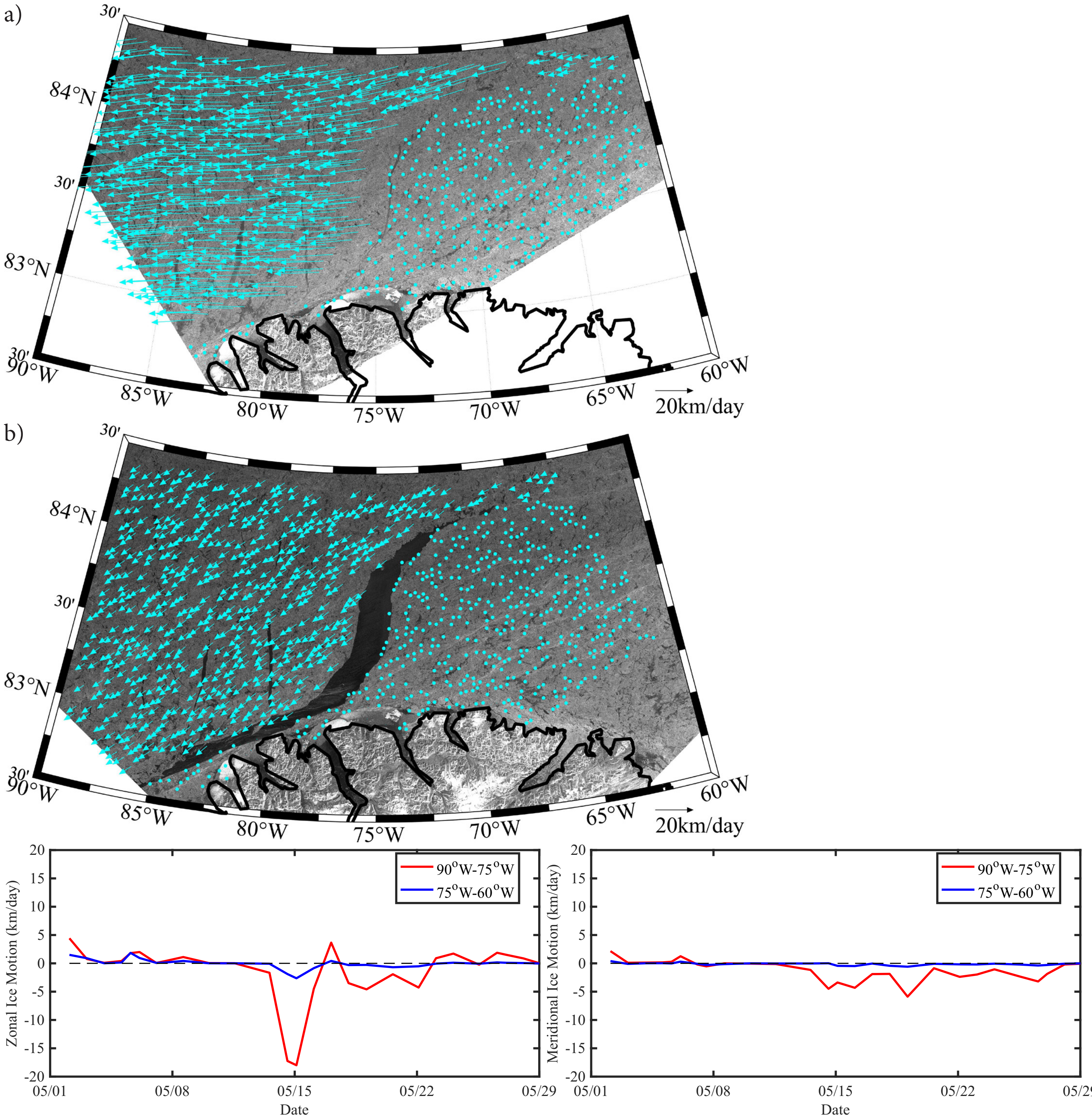

Figure 3) Sentinel-1 SAR imagery and ice motion during the May 2020 polynya event. SAR imagery and ice motion (km/day) on May: a) 14 and b) 15 2020. Time series of the: c) zonal and d) meridional components of the ice motion (km/day) over eastern (blue curves) and western (red curves) halves of the region of interest during May 2020.

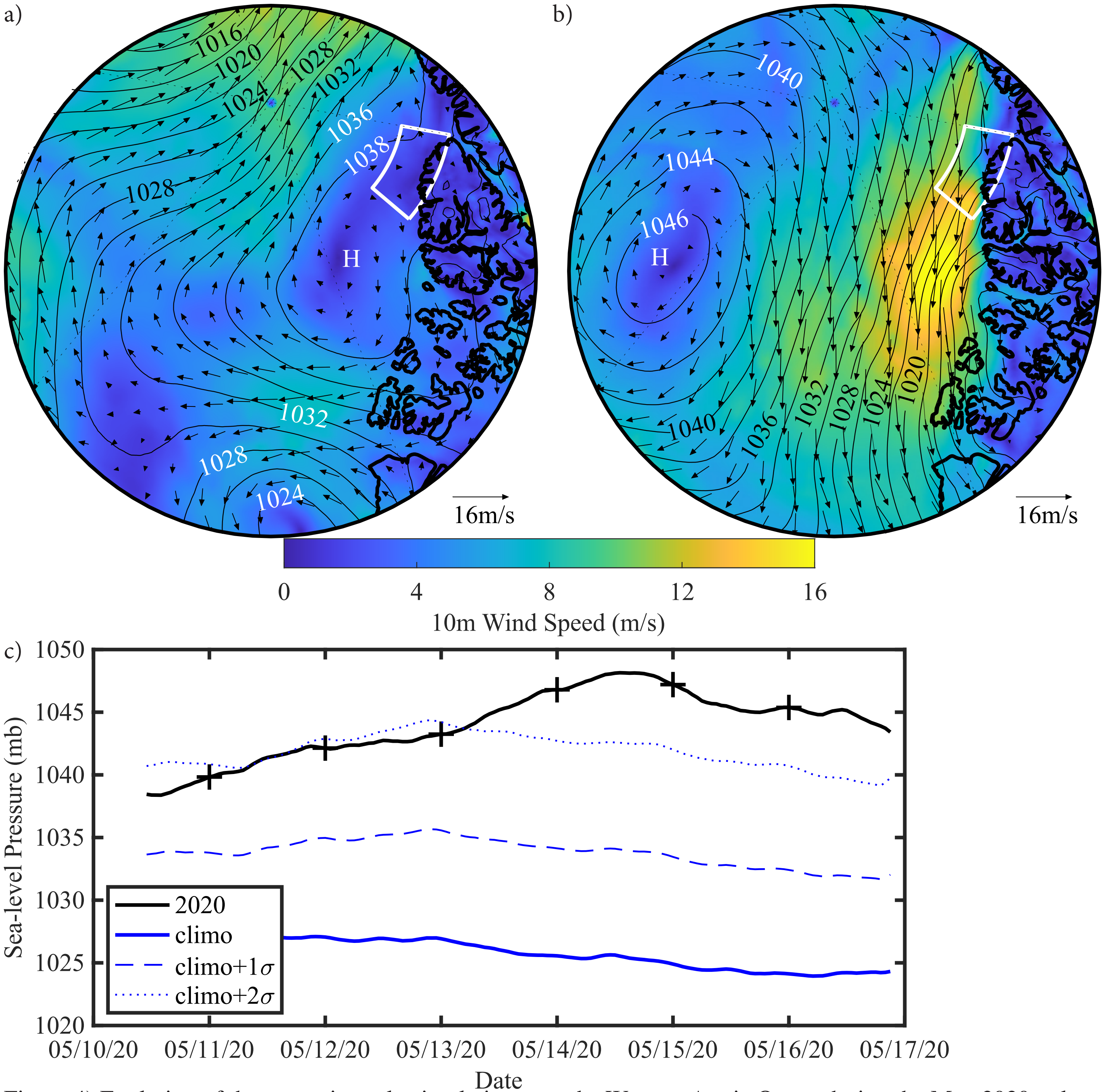

Figure 4) Evolution of the synoptic-scale circulation over the Western Arctic Ocean during the May 2020 polynya event. Sea-level pressure (mb-contours), 10m winds (m/s-vectors) and 10m wind speed (m/s-shading) from the ERA5 reanalysis at 00 GMT on May: a) 11 and b) 15 2020. c) The time series (black curve) of the central pressure of the high-pressure system identified in a) and b) with the climatology (blue curves) based all grid points within 500 km of the center of the high-pressure system during the period 1950-2020. In a) and b), the region of interest is indicated by the polygon.

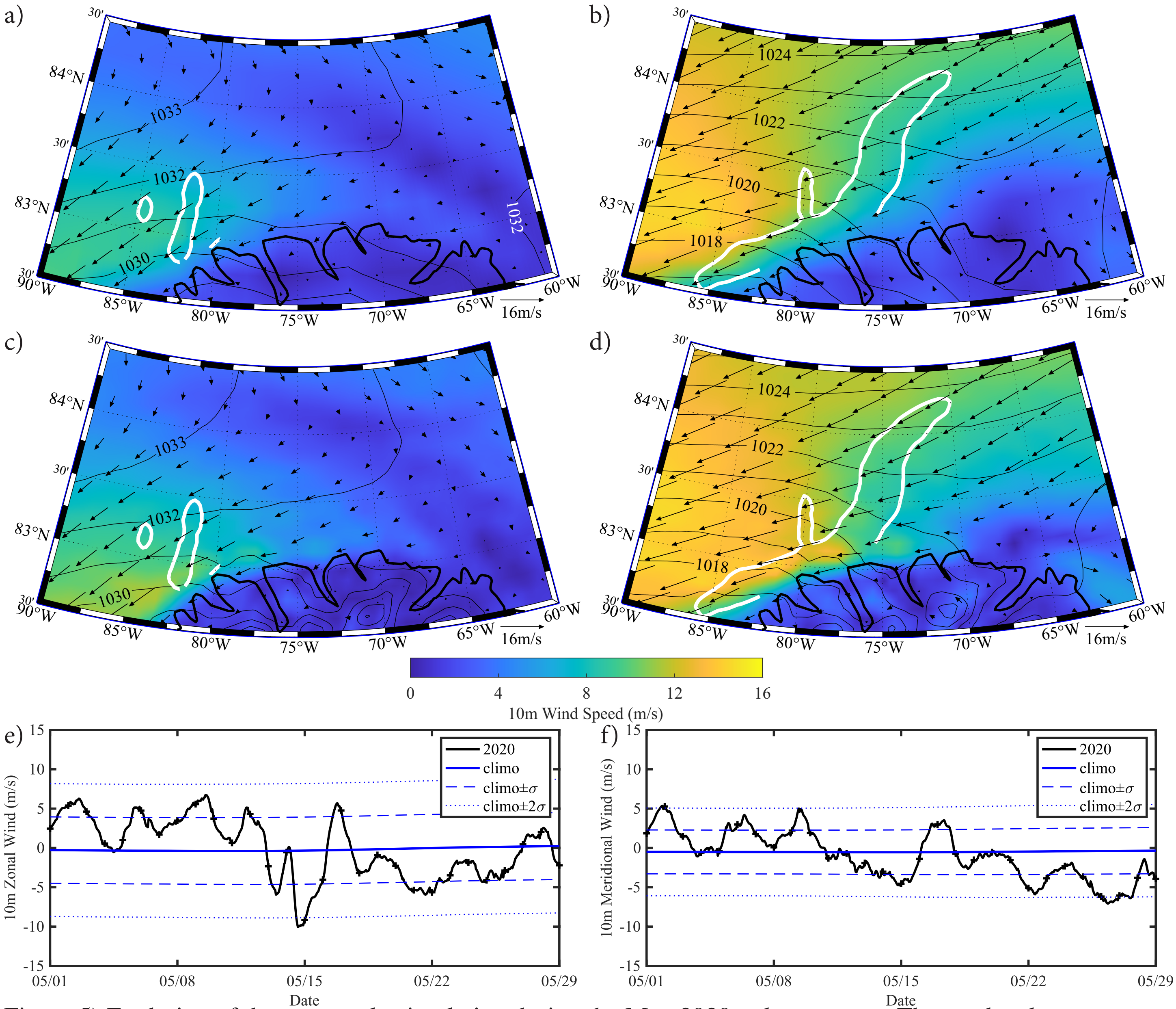

Figure 5) Evolution of the mesoscale circulation during the May 2020 polynya event. The sea-level pressure (mb-contours), the 10m wind (m/s-vectors) and the 10m wind speed (m/s shading) at 00 GMT May 14 2020 from the: a) ERA and b) ECOA and at 00 GMT May 15 2020 from the: c) ERA5 reanalysis and d) ECOA. Also shown with the white contours is the 80% sea ice concentration isocontour from the ASI dataset. The time series of the: a) zonal and c) meridional components of the 10m wind from the ERA5 reanalysis during May 2020 for the oceanic portion of the region of interest. The climatology is based on 1950-2020.

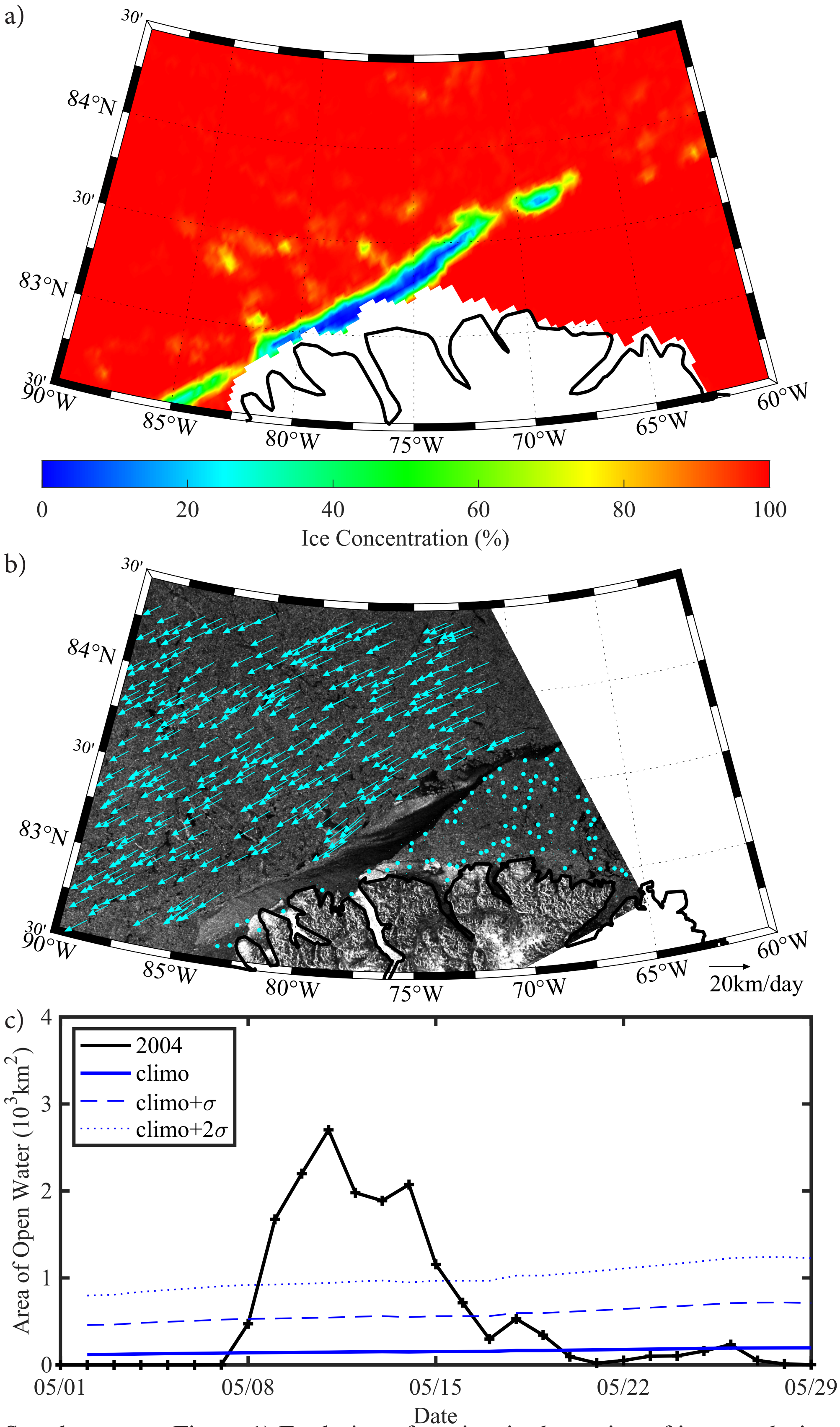

Supplementary Figure 1) Evolution of sea ice in the region of interest during the May 2004 polynya event north of Ellesmere Island. a) Sea ice concentration (%) from the ASI dataset on May 10 2004. b) SAR imagery and ice motion (km/day) on May 11 2004. c) Time series (black curve) of the area of open water (10^3 km^2) in the region of interest during May 2004, the climatology (blue curves) is based on 2003-2021.

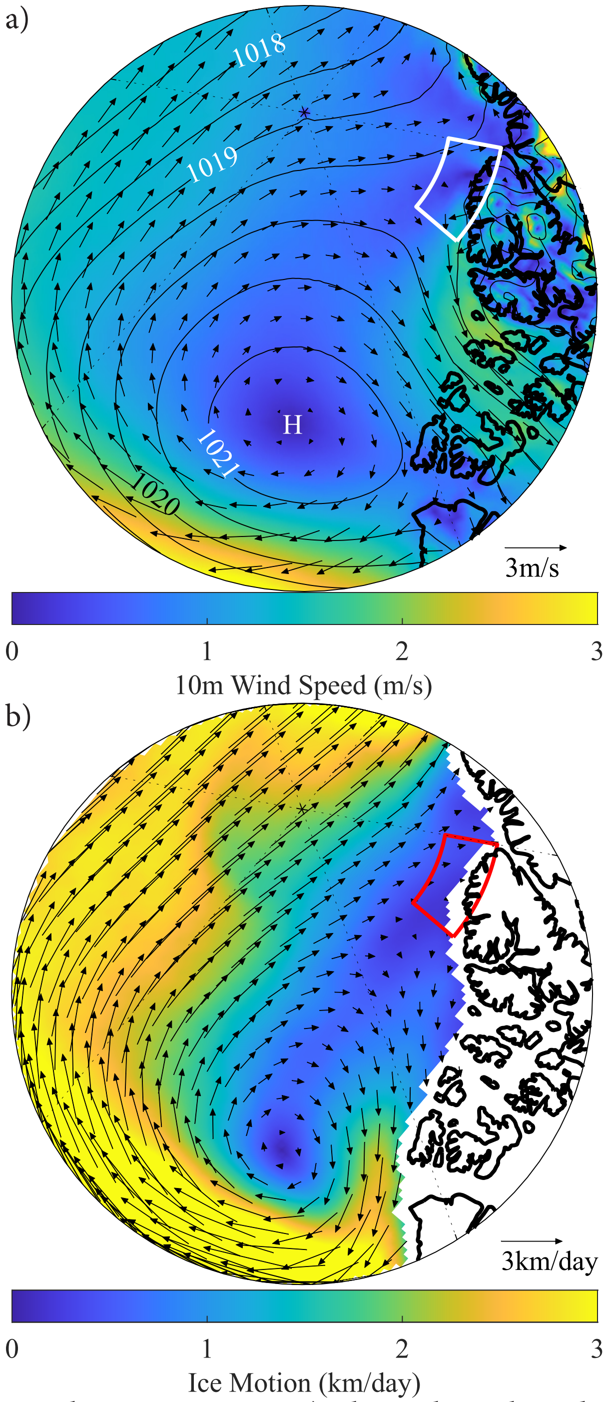

Supplementary Figure 2) Climatological conditions in the western Arctic during May. a) sea-level pressure (mb-contours), 10 winds (m/s-vectors) and 10m wind speed (m/s-shading) from ERA5 1950-2020. b)Sea ice motion (km/day) from the NSIDC dataset 1979-2018; The region of interest is indicated by the polygon.

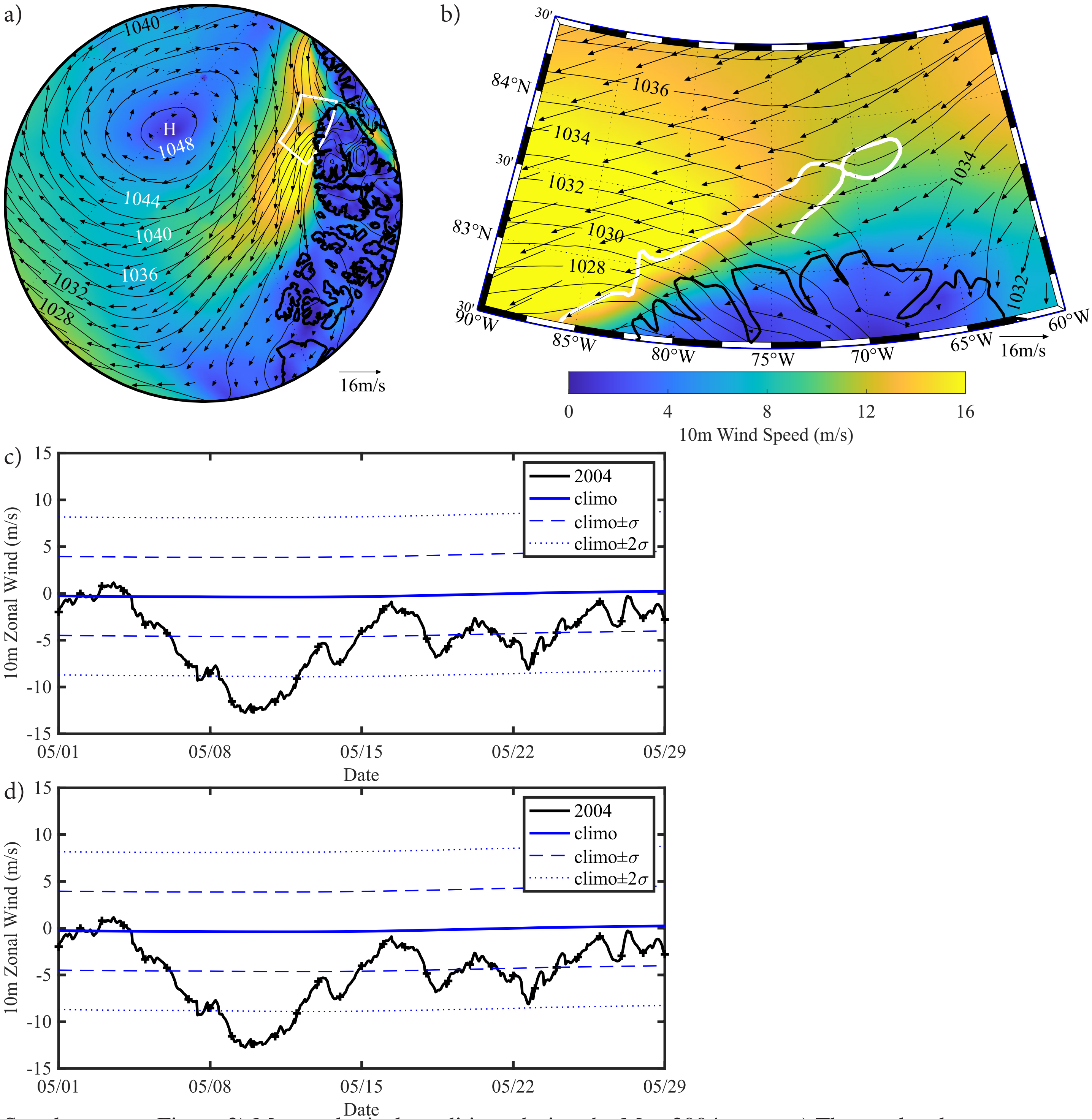

Supplementary Figure 3) Meteorological conditions during the May 2004 event. a) The sea-level pressure (mb-contours), the 10m wind (m/s-vectors) and the 10m wind speed (m/s shading) at 00 GMT May 10 2004 from the ERA5 reanalysis b) Same as a) except for the region of interes. Also shown in a) and b) with the white contours is the 80% sea ice concentration isocontour from the ARTIST dataset. The time series (black curves) of the: a) zonal component and c) meridional component of the 10m wind from the ERA5 reanalysis during May 2004 for the oceanic region bounded by 82.5°N and 84.5°N and 90°W and 60°W. The climatology is based on 1950-2020.